

# Robust Torque-Observed Control with Safe Input–Output Constraints for Hydraulic In-Wheel Drive Systems in Mobile Robots

Mehdi Heydari Shahna<sup>a,\*</sup>, Pauli Mustalahti<sup>a</sup>, Jouni Mattila<sup>a</sup>

<sup>a</sup>Faculty of Engineering and Natural Sciences, Tampere University, Tampere, 33720, Finland

## Abstract

Hydraulic-powered in-wheel drive (IWD) mechanisms enhance the maneuverability, traction, and maintenance efficiency of heavy-duty wheeled mobile robots (HWMRs) by enabling independent operation of each wheel. However, these highly nonlinear and multi-component systems are prone to instability and can endanger their surrounding environment due to failures imposed by faulty sensors and wheel slip on rough terrains. To design a robust synchronous control strategy for distributed hydraulic-powered IWD-actuated HWMR systems against such challenges in uncertain and time-varying operating conditions, this paper proposes a novel robust torque-observed valve-based control (RTOVC) framework for each independent hydraulic-powered IWD-actuated wheel of HWMRs, guaranteeing robustness and uniformly exponential stability of the entire system. To lay the groundwork for achieving this, a robust torque observer network based on an adaptive barrier Lyapunov function (BLF) is proposed to estimate the required wheel/motor torque, ensuring that the actual velocities of the IWD-actuated wheel align with the reference values in motion dynamic frames. It eliminates the closed-loop dependency in the control system associated with fault-prone torque (or hydraulic pressure) sensors. Then, an adaptive BLF-based valve control in the hydraulic system is employed to modulate the hydraulic fluid to generate the observed torque for each IWD-actuated wheel. The RTOVC framework reduces the risk of faults in hydraulic IWD-actuated HWMRs by constraining input-output key signals—such as valve control signals, actual wheel velocities, tracking errors, and motor/wheel torques—within the logarithmic BLF framework, ensuring they remain within safe limits. A thorough experimental analysis on a 6,500-kg hydraulic-powered IWD-actuated HWMR across rough terrains, where failures may occur due to severe slipping conditions and hydraulic system uncertainties, confirms the RTOVC's robust performance compared with two other state-of-the-art control strategies.

**Keywords:** Robust control, wheeled mobile robot, distributed systems, hydraulic systems, fault-tolerant control.

## Nomenclature

The following abbreviations and symbols will be used in the forthcoming equations.

### Abbreviations

<b>IWD</b>	Hydraulic in-wheel drive
<b>HWMR</b>	Heavy-duty wheeled mobile robots HWMR
<b>RTOVC</b>	Robust torque-observed valve-based control
<b>BLF</b>	Barrier Lyapunov function
<b>LWMR</b>	Light-duty wheeled mobile robot
<b>RL</b>	Rear left wheel (number 1)
<b>RR</b>	Rear right wheel (number 2)
<b>FL</b>	Front left wheel (number 3)
<b>FR</b>	Front right wheel (number 4)
<b>BAC</b>	Backstepping-based adaptive control
<b>DVSC</b>	Decentralized-valve-structure control

**PID** Proportional–integral–derivative

### Wheel Motion Dynamics

$D_1$	Slippage disturbances of the wheel
$F_1$	Uncertainties of the wheel
$F_\omega$	Vertical normal force of the wheel
$G_1$	Known modeling term of the wheel
$J_\omega$	Wheel inertia
$\omega_\omega$	Actual angular velocity of the wheel
$\tau_\omega$	Wheel torque
$a_1$	Unknown positive coefficient of the wheel torque
$c_\omega$	Damping coefficient
$d_\omega$	Disturbances of the wheel
$f_\omega$	Coulomb's friction of the rotation shaft of the wheel
$r$	Wheel radius
$s_\omega$	Slip ratio of the wheel
$v_\omega$	Linear velocity of the wheel

### Hydraulic-Powered IWD System Parameters

$\tau_m$  Hydraulic in-wheel motor torque

\*Corresponding author: Mehdi Heydari Shahna  
E-mail address: mehdi.heydarishahna@tuni.fi

$m_\omega$	Gear ratio of each wheel	$v_{max}$	Bound of the desired linear velocity: $v_d \leq  v_{max} $
$p_T$	Tank pressure or return pressure	$Q_1$	A positive notation: $Q_1 = \alpha_1^2 - v_e^2$
$p_s$	Source pressure provided by the hydraulic pump	$\alpha_1$	Bound of velocity tracking error: $v_e <  \alpha_1 $
$Q_A$	Flows provided by the hydraulic valve at point A	$\beta_1$	A positive notation: $\beta_1 = \frac{v_e}{Q_1}$
$Q_B$	Flows provided by the hydraulic valve at point B	$\hat{\psi}_1$	Adaptive parameter of the first law
$p_A$	Pressure at point A	$\psi_1^*$	Positive constant: the target of the first adaptive law
$p_B$	Pressure at point B	$\tilde{\psi}_1$	The error of the first adaptive law: $\tilde{\psi}_1 = \hat{\psi}_1 - \psi_1^*$
$\omega_m$	Angular velocity of hydraulic motor	$k_2$	Positive constant: Adaptive design parameter
$V_A$	Volume of fluid per revolution at point A	$k_3$	Positive constant: Adaptive design parameter
$V_B$	Volume of fluid per revolution at point B	$k_4$	Positive constant: Adaptive design parameter
$V_m$	Volume of fluid per revolution	$D_1^*$	Unknown positive constant: $\ D_1\  \leq D_1^*$
$\Delta p$	Pressure difference	$Q_2$	A positive notation: $Q_2 = \tau_{max}^2 - \hat{\tau}_m^2$
$\eta_{hm}$	Hydromechanical inefficiencies	$V_1$	A logarithm-based BLF: $V_1 = \frac{1}{a_1} \Theta_1 + \frac{1}{k_3} \tilde{\psi}_1^2$
$\eta_{vol}$	Volumetric inefficiencies	$\Omega_{11}$	Positive constant: $\Omega_{11} = \min[a_1 k_1, k_3 k_4]$
$\gamma$	Effective bulk modulus of the hydraulic system	$\Omega_{12}$	Positive constant: $\Omega_{12} = \frac{1}{4} \rho_2^{-1} + \frac{1}{2} k_4 \psi_1^{*2}$
$Q$	Load flow of the hydraulic system	$\beta_2$	A positive notation: $\beta_2 = \frac{\hat{\tau}_m}{Q_2}$
$x_u$	Normalized spool position of valves	$\hat{\psi}_2$	Adaptive parameter of the second law
$K_u$	Flow coefficient of the valve	$\hat{\tau}_\omega$	Estimation of the wheel torque
$u$	Valve control signal	$\mu_1$	Unknown positive constant: $\ F_1^*\  \leq \mu_1 m_1$
Sat( $u$ )	Functional Constraint on valve control signal	$\psi_2^*$	Positive constant: the target of the second adaptive law
$\bar{u}$	Upper nominal valve control signal	$\rho_1$	Any positive constant
$\underline{u}$	Lower nominal valve control signal	$\rho_2$	Any positive constant
$\lambda_1$	A function between 0 and 1	$\tilde{\psi}_2$	The error of the second adaptive law: $\tilde{\psi}_2 = \hat{\psi}_2 - \psi_2^*$
$D_2$	Unknown external disturbances in the hydraulic system	$k_1$	Positive constant: torque observer design parameter
$F_2$	Uncertainties in the hydraulic system	$k_7$	Positive constant: Adaptive design parameter
$\lambda_2$	A positive function: $0 \leq \lambda_2 \leq \max( \underline{u} +1,  \bar{u} +1)$	$k_8$	Positive constant: Adaptive design parameter
$a_2$	Unknown valve control signal coefficient	$k_9$	Positive constant: Adaptive design parameter
<i>RTOVC Framework Parameters</i>			
$C$	Any defined region in stability concept	$m_1$	Unknown continuously positive function: $\ F_1^*\  \leq \mu_1 m_1$
$F_1^*$	Unknown function: $F_1^* = F_1 - \dot{v}_d$	$D_2^*$	Unknown positive constant: $\ D_2\  \leq D_2^*$
$Y$	Any state of a system	$V_2$	A logarithm-based BLF: $V_2 = \frac{1}{a_2} \Theta_2 + \frac{1}{k_8} \tilde{\psi}_2^2$
$\bar{b}$	Positive constant	$\Omega_{21}$	Positive constant: $\Omega_{21} = \min[a_2 k_2, k_8 k_9]$
$\bar{c}$	Positive constant	$\Omega_{22}$	Positive constant: $\Omega_{22} = \frac{1}{4} \rho_4^{-1} + \frac{1}{2} k_9 \psi_2^{*2}$
$\epsilon_1$	Bound of the actual linear velocity: $v_\omega \leq  \epsilon_1 $	$\mu_2$	Unknown positive constant: $\ F_2^*\  \leq \mu_2 m_2$
$\omega_d$	Desired angular velocity of each wheel	$\rho_3$	Any positive constant
$\omega_e$	Angular velocity error of each wheel: $\omega_e = \omega_\omega - \omega_d$	$\rho_4$	Any positive constant
$\tau_{max}$	Bound of the motor torque: $\tau_m <  \tau_{max} $	$k_6$	Positive constant: valve control design parameter
$\zeta$	Positive constant	$m_2$	Unknown continuously positive function: $\ F_2^*\  \leq \mu_2 m_2$
$k_5$	Positive constant, satisfying $k_5 \geq J_\omega = a_1^{-1}$	$E_0$	A non-decreasing function: $E_0 = \Theta_i^2 e^{\bar{i}(w-t_0)}$
$t$	Time	$E_1$	A function: $E_1 = \sup_{w \in [t_0, t]} \left[ \sum_{i=1}^2 \rho_{2i-1}^{-1} \left( m_i^2 \right) e^{\bar{i}(w-t_0)} \right]$
$t_0$	Initial time	$Z(t)$	A positive continuous operator: $Z(t) = \frac{0.5}{\Omega-t}$
$v_d$	Desired linear velocity of each wheel	$\Omega$	A positive constant: $\Omega = \min[\Omega_{11}, \Omega_{21}]$
$v_e$	Linear velocity error of each wheel: $v_e = v_\omega - v_d$	$\Theta_i$	A logarithmic function for $i = 1, 2$ : $\Theta_i = \log\left(\frac{\alpha_i^2}{Q_i}\right)$

$\alpha_2$	Bound of the motor torque: $\alpha_2 = \tau_{max}$
$\bar{E}$	A non-decreasing function: $\bar{E} = \max[E_0, E_1]$
$\bar{V}$	A logarithm-based BLF: $\bar{V} = V_1 + V_2$
$\bar{\Omega}$	A positive constant: $\bar{\Omega} = \Omega_{12} + \Omega_{22}$
$\iota$	A positive constant: $0 \leq \iota < \Omega$
$\iota^*$	A positive constant: $\bar{\iota} < \iota^* < \Omega$
$\bar{Z}$	A positive continuous operator: $\bar{Z} = Z(\iota^*)$
$w$	A positive constant: $t_0 \leq w \leq t$
$\bar{V}$	A logarithm-based BLF: $\bar{V} = \sum_{j=1}^4 \bar{V}_j$
$g_0$	A defined region of stability for any IWD
$j$	Number of each wheel: $j = 1, \dots, 4$
$\tau_0$	The radius of the region $g_0$
$\Omega_j$	A positive constant: $j$ th wheel's $\Omega$
$\bar{V}_j$	A logarithm-based BLF: $j$ th wheel's $\bar{V}$
$\bar{\Omega}_j$	A positive constant: $j$ th wheel's $\bar{\Omega}$
$\tilde{\Omega}$	A positive constant: $\tilde{\Omega} = \min\{\Omega_j \mid j = 1, \dots, 4\}$
$\tilde{\bar{\Omega}}$	A positive constant: $\tilde{\bar{\Omega}} = \sum_{j=1}^4 \bar{\Omega}_j$
$\Theta_{i,j}$	A logarithmic function: $j$ th wheel's $\Theta_i$ with $i = 1, 2$
$\rho_{2i-1,j}$	Any positive constant
$m_{i,j}$	Unknown positive function: $j$ th wheel's $m_i$ for $i = 1, 2$
$\tilde{g}_0$	A defined region of stability for the HWMR
$\bar{\tau}_0$	The radius of the region $\tilde{g}_0$

## 1. Introduction

An in-wheel drive (IWD) system with its own motor equips each wheel of a four-wheel distributed vehicle system, enabling independent power delivery and enhanced responsiveness to various road conditions [1, 2]. IWD systems eliminate traditional mechanical components of vehicles, such as differentials, by utilizing individual controllers for precise torque distribution, resulting in improved traction, reduced maintenance, and simplified motor replacements [3]. This technology applies to diverse machinery and mobility systems requiring high maneuverability, making them increasingly integral to the design and functionality of off-road vehicles, such as heavy-duty wheeled mobile robots (HWMRs).

Recently, HWMRs have been extensively employed due to their operational capabilities in various industrial circumstances in which it might be inefficient, dangerous, or impossible for humans to work [4, 5]. In applications such as construction, manufacturing, aerospace, and mining, many drive systems of HWMRs rely on hydraulic servomechanisms due to their power density and high torque at low speeds [6]. This makes them more shock-resistant and suitable for handling high loads effectively [7].

Unfortunately, the safety and stability of HWMRs on rough terrain are compromised by wheel slippage, caused by terrain

variations, load distribution imbalances, poor wheel design, dynamic forces during movement, and limitations in the robot's control systems, which may be incapable of making timely adjustments. Surprisingly, over the past twenty years, studies addressing wheel slippages among HWMRs have had relatively little focus, with less than 6% of total publications on HWMRs [8].

A comprehensive literature review was conducted using the keywords 'hydraulic motor,' 'wheel,' 'off-road,' 'tracking,' and 'control.' The search strategy involved querying Google Scholar and other academic databases to ensure an exhaustive review of relevant literature. The results of the literature review are summarized in Fig. 1, which illustrates the distribution of research on the control of hydraulic motor-driven HWMRs since 2020. According to our findings, the number of studies on hydraulic motor-driven HWMRs has notably increased in recent years, influenced by autonomous trends in heavy-duty industries, but there is still a significant shortage of robust control systems with proven stability for these high-power robots to address wheel slippages, whose development is vital to advancing the field [9, 10].

To compensate for wheel slippages in complex off-road drive systems, tracking velocity-based control has minimal computational complexity [8, 11]. However, the wheel torque in this control strategy tends to be generated excessively [8, 11], leading to soil terrain failure [8] and a harmful increase in the generation of other key signals, such as valve control, tracking error, and actual velocity of each hydraulic IWD. This excessive torque may pose threats to adjoining facilities, compromise the system's mobility, and lead to failures. Therefore, it is essential to impose safe constraints on key signals to reduce the risk of system instability and faults in hydraulic-powered, IWD-actuated HWMRs operating in uncertain and time-varying conditions.

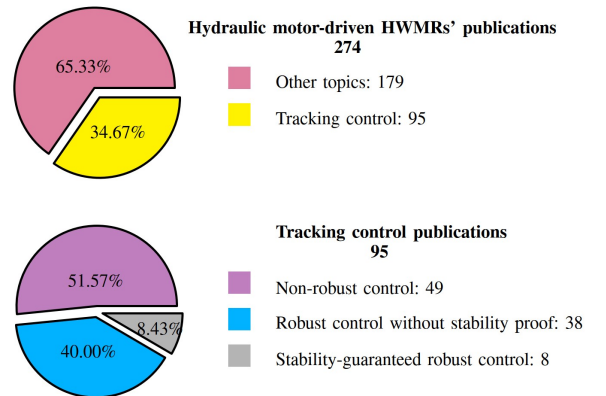


Fig. 1. Distribution of hydraulic-powered HWMRs research with various motor configurations since 2020.

In addition, controlling hydraulic servomechanisms conventionally requires numerous fault-prone sensors. For instance, feedback torque/pressure information, either directly by using a motor torque/force sensor or indirectly through calculations based on pressure sensors for opening valves is required to generate sufficient torque efforts applied to in-wheel motors [12].

However, incorporating such sensors not only increases the cost of designing an HWMR but also renders the control system more dependent on sensors that are susceptible to faults in a harsh environment with heavy loads [13, 14].

To address robustness against such challenges for HWMRs in uncertain and time-varying operating conditions, research studies documented in [15, 16, 17, 18] consistently emphasized on tracking control, managing modeling uncertainties, and mitigating external disturbances. In addition, further advancements reported by [19, 20, 21] took steps forward by addressing safety constraints in certain aspects, thereby broadening the scope and applicability of these control strategies. However, it is still required to achieve further advancements in designing a strongly stability-guaranteed, safe, and robust control system that decreases the closed-loop dependency associated with fault-prone sensors specifically for valve-based IWD-actuated HWMRs.

It is beyond doubt that key control signals of IWD-actuated HWMRs must safely be constrained within predefined safety limits to prevent system faults, minimize wheel slippage, and enhance operational safety in environments characterized by highly uncertain and unstructured conditions, but incorporating these safety constraints into the control system, while simultaneously ensuring both robustness and stability, remains the primary challenge.

As a solution in control theory, a barrier Lyapunov function (BLF) control extends the traditional Lyapunov concept, primarily focused on the stability or convergence of system states, by incorporating constraints that the system should never violate [22, 23]. This capability has led to more research studies on BLF-based control for various applications. Specifically, our literature search included querying Google Scholar and other academic databases that used the keywords ‘Barrier Lyapunov Function,’ ‘control,’ and ‘motor,’ revealed that the number of publications containing these keywords since 2020 has tripled compared to that from 2010 to 2020. Fig. 2 shows the number of BLF-based control studies for various applications utilizing motor-driven actuators, including HWMRs, light-duty wheeled mobile robots (LWMRs), and other applications since 2020. These results demonstrate that the capabilities of BLF in HWMR control have not yet been fully realized. All seventeen BLF-based control publications cannot apply to our case study, which involves highly nonlinear hydraulic-powered IWD-actuated HWMR systems prone to sensor faults and severe wheel slippage.

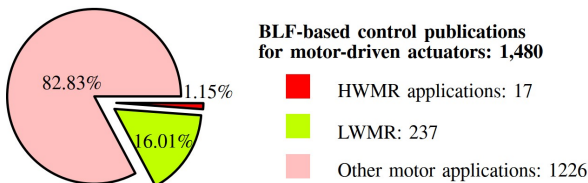


Fig. 2. Distribution of BLF-based control research for motor-driven actuators with any power type Since 2020.

This paper proposes a novel robust torque-observed valve-based control (RTOVC) framework for independently IWD-

actuated HWMR platforms. To begin with, a new torque observer is designed based on the adaptive BLF to estimate the necessary torque to align the wheel velocity with the reference one and effectively reject the imposed disturbances due to rough terrains, wheel slippage, and other wheel effects. Concurrently, the estimated torque is fed into another adaptive BLF, which regulates valve control signals to modulate the hydraulic pressure to either increase or decrease the force exerted by the hydraulic fluid to achieve the estimated torque for each actuator. As a summary, this work provides the following new findings in the field:

(1) to eliminate the closed-loop dependency in the control system associated with fault-prone torque (or hydraulic pressure) sensors, a novel robust IWD-actuated wheel torque observer is introduced in the RTOVC framework;

(2) to address the issue of excessive torque generation, a common problem in velocity-based control systems, particularly during wheel slippage, the hydraulic motor torque is safely constrained within a logarithmic BLF framework;

(3) to reduce the risk of system faults occurring in IWD-actuated HWMRs, other key input-output signals—such as the actual velocity and tracking errors of IWD-actuated wheel and valve control signals—are constrained within another logarithmic BLF framework;

(4) the RTOVC-applied IWD-actuated wheels contribute to the robustness and stability of the entire distributed HWMR system into a specified stable region with an exponential convergence rate. The radius of the stable region adaptively depends on the intensity of slippage, load, and rough terrain effects.

The remainder of this paper is organized as follows: the modeling formulation of each valve-based IWD mechanism of HWMRs is investigated in Section 2, where the effect of wheel slippage and different forces on wheels in mathematical terms are discussed and the hydraulic in-wheel motors are modeled. Then, the mathematical effects of valve signal constraints on the hydraulic-powered IWD dynamic system are demonstrated. Section 3 presents the step-by-step design of the RTOVC, ensuring the uniformly exponential stability of the RTOVC-applied hydraulic servomechanism for each wheel of an HWMR, and consequently, the stability of the entire system. Finally, Section 4 demonstrates the validity of the RTOVC strategy by presenting a comprehensive experiment on a 6,500-kg hydraulic-powered IWD-actuated HWMR across two challenging terrains: (1) snow-covered gravel terrain with soft soil and (2) ice-covered stony terrain with an approximate slope of 35 degrees.

## 2. Hydraulic-powered IWD-actuated wheel model of HWMRs

### 2.1. Motion dynamic formulation of each the wheel under slippage and uncertainties

Normally, the tractive force generated by each wheel on a surface propels an HWMR forward by overcoming various resistances. This force is directly related to the torque received

from the in-wheel driving gear (hydraulic motor)  $\tau_m$  and is converted into the driven gear (wheel)  $\tau_\omega$ . The linear dynamics of each driving wheel under slippage can be provided, as [24, 25]:

$$\dot{v}_\omega = \frac{r}{J_\omega} (\tau_\omega - rF_\omega - c_\omega\omega_\omega - f_\omega + d_\omega) - \dot{s}_\omega \quad (1)$$

where  $v_\omega$  and  $\omega_\omega$  are the linear angular velocities of each wheel. The damping coefficient is represented as  $c_\omega$ , and the Coulomb's friction of the rotation shaft  $f_\omega$  ( $\omega_\omega$ ).  $d_\omega$  represents the disturbance,  $F_\omega$  is the vertical normal force of each wheel,  $J_\omega$  is the wheel inertia, and  $r$  is the wheel radius. The wheel slip for IWDs is defined as an unknown function  $s_\omega$ . We simplify them, as follows:

$$\dot{v}_\omega = a_1\tau_\omega + G_1(\omega_\omega, v_\omega) + F_1(\omega_\omega, v_\omega) + D_1(t) \quad (2)$$

where  $G_1$  is assumed the known modeling term,  $a_1$  is an unknown positive coefficient,  $F_1$  represents the unknown modeling error due to uncertainties, and  $D_1$  represents external disturbances due to the wheel slippage.

## 2.2. Hydraulic-powered IWD formulation under system uncertainties

The valve-based servomechanism based on [26, 27] for each wheel can be modeled. An HWMR actuated by four independently valve-controlled IWDs is illustrated in Fig. 3. Note that  $p_T$  is the tank pressure or return pressure,  $p_s$  is the source pressure provided by one hydraulic pump (supplying energy to the four-wheel systems),  $Q_A$  and  $Q_B$  are the flows provided by the hydraulic control valves,  $p_A$  and  $p_B$  are pressures at different points in the hydraulic system,  $\omega_m$  is the angular velocity of the hydraulic motor.

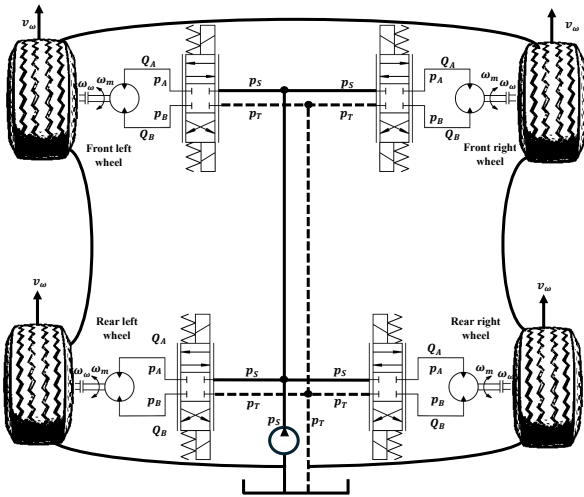


Fig. 3. A four hydraulic-powered IWD-actuated HWMR with independent valve control.

Each in-wheel motor torque can be generated as the pressure difference between the high-pressure line and low-pressure line, as [27]:

$$\tau_m = \Delta p \frac{V_m}{2\pi} \eta_{hm} \quad (3)$$

where we assume both line volumes are equal to the motor displacement  $V_A = V_B = V_m$  (volume of fluid per revolution) and  $\Delta p = p_A - p_B$ . We assume  $\eta_{hm}$  demonstrates unknown hydromechanical inefficiencies. The differential pressure dynamic of the hydraulic motor based on the control valve flow can be provided as [27, 28]:

$$\Delta \dot{p} = \frac{\gamma}{V_m} \left( Q - \omega_m \frac{V_m}{\pi} \eta_{vol} \right) \quad (4)$$

We assume volumetric inefficiencies  $\eta_{vol}$  such as internal leakage, slightly may exist and are unknown.  $\gamma$  is the effective bulk modulus of the system, and  $Q = Q_A - Q_B$  is the load flow. The inverse flow-pressure dynamics of motors can be provided as in [27, 28]:

$$Q = \dot{\tau}_m \frac{2\pi}{\gamma \eta_{hm}} + \omega_m \frac{\gamma V_m}{\pi} \eta_{vol} \quad (5)$$

By inverse mapping the control signal valve, we know [27]:

$$u = \frac{Q}{K_u \sqrt{2(p_s - \text{sign}(x_u) \Delta p)}} \quad (6)$$

where  $x_u$  is the normalized spool position,  $K_u$  is the flow coefficient of the valve,  $u$  is the valve control signal, and:

$$\text{sign}(x_u) = \begin{cases} -1 & \text{if } x_u < 0, \\ 0 & \text{if } x_u = 0, \\ 1 & \text{if } x_u > 0. \end{cases} \quad (7)$$

From (3-6), we obtain the differential motor torque, as:

$$\dot{\tau}_m = \frac{\gamma \eta_{hm} K_u}{2\pi} \sqrt{2(p_s - \text{sign}(x_u) \Delta p)} u - \omega_m \frac{\gamma^2 V_m \eta_{hm} \eta_{vol}}{2\pi^2} \quad (8)$$

This study assumes all valve-based servomechanism parameters of (8) are unknown. To constrain the valve control signals for each servomechanism of the wheel, we should have:

$$\text{Sat}(u) = \begin{cases} \bar{u}, & u \geq \bar{u} \\ u & \underline{u} \leq u \leq \bar{u} \\ \underline{u} & u \leq \underline{u} \end{cases} \quad (9)$$

where  $\bar{u}$  and  $\underline{u}$  specify the upper and lower nominal valve control signals, respectively. Consequently, we define:

$$\text{Sat}(u) = \lambda_1 u + \lambda_2 \quad (10)$$

where

$$\lambda_1 = \begin{cases} \frac{1}{|u|+1}, & u \geq \bar{u} \text{ or } u \leq \underline{u} \\ 1 & \underline{u} < u < \bar{u} \end{cases} \quad (11)$$

and

$$\lambda_2 = \begin{cases} \bar{u} - \frac{u}{|u|+1}, & u \geq \bar{u} \\ 0 & \underline{u} < u < \bar{u} \\ \underline{u} - \frac{u}{|u|+1} & u \leq \underline{u} \end{cases} \quad (12)$$

Eqs. (10), (11), and (12) imply Eq. (9). Note  $0 \leq \lambda_2 \leq \max(|\underline{u}|+1, |\bar{u}|+1)$  and  $0 \leq \lambda_1 \leq 1$ . Thus, by considering (9), we will have (8) as the following form:

$$\dot{\tau}_m = \frac{\gamma \eta_{hm} K_u}{2\pi} \sqrt{2(p_s - \text{sign}(x_u) \Delta p)} \text{Sat}(u) - \omega_m \frac{\gamma^2 V_m \eta_{hm} \eta_{vol}}{2\pi^2} \quad (13)$$

From (10) and (13):

$$\begin{aligned} \dot{\tau}_m = & \frac{\gamma\eta_{hm}K_u}{2\pi} \sqrt{2(p_s - \text{sign}(x_u)\Delta p)\lambda_1} u \\ & + \frac{\gamma\eta_{hm}K_u}{2\pi} \sqrt{2(p_s - \text{sign}(x_u)\Delta p)\lambda_2} - \omega_m \frac{\gamma^2 V_m \eta_{hm} \eta_{vol}}{2\pi^2} \end{aligned} \quad (14)$$

Similar to (2), let us to simplify (14), as follows:

$$\dot{\tau}_m = a_2 u + F_2(\omega_\omega) + D_2 \quad (15)$$

where  $a_2$  is an unknown positive coefficient,  $F_2$  represents the unknown modeling term due to uncertainties in the hydraulic system, and  $D_2$  represents external disturbances.

### 3. Design of RTOVC Framework for each hydraulic-powered IWD-actuated wheel of the HWMR

#### 3.1. Problem Formulation and safety constraints

The tracking error of each wheel is introduced, as follows:

$$v_e(t) = v_\omega(t) - v_d(t), \quad \omega_e(t) = \frac{v_e(t)}{r} = \omega_\omega(t) - \omega_d(t) \quad (16)$$

where  $\omega_e$  and  $v_e$  are the tracking angular and linear velocity error of the wheel between the actual angular/linear ( $\omega_\omega$  or  $v_\omega$ ) and reference ( $\omega_d$  or  $v_d$ ) velocity of the wheel. By considering (2), and making a derivative of (16) for linear velocity error, we will have:

$$\dot{v}_e(t) = a_1 \tau_\omega(t) + G_1(\omega_\omega, v_\omega) + F_1(\omega_\omega, v_\omega) + D_1(t) - \dot{v}_d(t) \quad (17)$$

Let us define  $F_1^*(\omega_\omega, v_\omega, \dot{v}_d) = F_1(\omega_\omega, v_\omega) - \dot{v}_d(t)$ . Thus:

$$\dot{v}_e(t) = a_1 \tau_\omega(t) + G_1(\omega_\omega, v_\omega) + F_1^*(\omega_\omega, v_\omega, \dot{v}_d) + D_1(t) \quad (18)$$

Assume the reference linear velocity is bounded, as  $|v_d| \leq v_{max}$  where  $v_{max}$  is a positive constant. After introducing the valve control signal constraint (system input constraint) in (9), let us apply safety-defined wheel constraints on actual linear velocity, tracking error, and motor/wheel torque, as follows:

$$|v_\omega| \leq \epsilon_1, \quad |v_e| < \alpha_1, \quad \tau_m < \tau_{max} \quad (19)$$

where  $\tau_{max}$  is a positive constant that can be adjusted to lower values on different terrains to address the issue of excessive motor torque generation, a common problem in velocity-based control systems, particularly during wheel slippage.  $\epsilon_1$  and  $\alpha_1$  are also positive constants to satisfy these conditions:  $v_{max} < \epsilon_1$ ,  $\alpha_1 = \epsilon_1 - v_{max}$ .

**Definition 1.** According to [29, 30, 31], for  $t \geq t_0$ , any state  $Y$  converges uniformly and exponentially with an exponential rate of  $\bar{b}$  within a stable region  $C$  with a radius  $\zeta$ , if:

$$\|Y\| \leq \bar{c} e^{-\bar{b}(t-t_0)} \|Y(t_0)\| + \zeta \quad (20)$$

where  $\bar{c}$ ,  $\zeta$ , and  $\bar{b} \in \mathbb{R}^+$  are positive constants.  $Y(t_0)$  is any initial state value, and  $C$  can be defined when  $t \rightarrow \infty$ , as:

$$C := \{Y \mid \|Y\| \leq \zeta\} \quad (21)$$

#### 3.2. Robust torque Observer Network for wheel motion dynamics

First, let us define an adaptive law  $\hat{\psi}_1$ , based on [32]:

$$\dot{\hat{\psi}}_1 = -k_3 k_4 \hat{\psi}_1 + \frac{1}{2} k_2 k_3 \beta_1^2 \quad (22)$$

$k_2, k_3, k_4$  are positive constants.  $\beta_1$  is a positive notation and is defined as:

$$\beta_1 = \frac{v_e}{\alpha_1^2 - v_e^2} \quad (23)$$

As observed in (23), if  $|v_e(t_0)| < \alpha_1(t_0)$ , the velocity error must satisfy  $|v_e| < \alpha_1$ . Increasing  $v_e^2$  and reaching  $\alpha_1^2$  leads to singularities in the system. For instance, in many programming platforms, execution may stop due to a warning, such as ‘Infinity or NaN value encountered,’ when the computed value exceeds the system’s numerical limits. This characteristic is useful for ensuring that the tracking error variable does not exceed the bound  $\alpha_1$ , which could be unsafe or undesirable in a control context. Let us propose the estimation of the wheel torque ( $\hat{\tau}_\omega$ ), as follows:

$$\hat{\tau}_\omega = -\frac{1}{2}(k_1 v_e + k_2 \hat{\psi}_1 \beta_1) - k_5 G_1 \quad (24)$$

$k_1$  is a positive constant.  $k_5$  is also a positive constant. Let us define the error of adaptation law as:

$$\tilde{\psi}_1 = \hat{\psi}_1 - \psi_1^* \quad (25)$$

where  $\psi_1^*$  is an unknown positive constant. As  $a_1$  is a positive constant, let us introduce a logarithm-based BLF, as follows:

$$V_1 = \frac{1}{2a_1} \log\left(\frac{\alpha_1^2}{Q_1}\right) + \frac{1}{2k_3} \tilde{\psi}_1^2 \quad (26)$$

where  $Q_1 = \alpha_1^2 - v_e^2$ . Similar to (23), according to the properties of logarithms in (26),  $Q_1$  cannot be zero or negative.

**Theorem 1:** Consider the logarithm-based BLF provided in (26). By applying the proposed estimation of the wheel torque provided in (24) to the wheel motion dynamics provided in (2), the error of velocity tracking, under the constraints  $|v_\omega| < \epsilon_1$  and  $|v_e| < \alpha_1$ , uniformly exponentially converges into a stable region depending on the bound of uncertainties and intensity of wheel slippage.

*Proof:* See **Appendix A**.

#### 3.3. Robust valve control network for hydraulic-powered IWDs

From (24), we can obtain the estimated motor torque as:

$$\hat{\tau}_m = \frac{\hat{\tau}_\omega}{m_\omega} \quad (27)$$

where  $m_\omega$  is the gear ratio between the motor and the driven wheel. Similar to (22), let us introduce another adaptive law  $\hat{\psi}_2$ , as:

$$\dot{\hat{\psi}}_2 = -k_8 k_9 \hat{\psi}_2 + \frac{1}{2} k_7 k_8 \beta_2^2 \quad (28)$$

where  $k_7, k_8$ , and  $k_9$  are positive constants.  $\beta_2$  is a positive notation and is defined, as:

$$\beta_2 = \frac{\hat{\tau}_m}{\tau_{max}^2 - \hat{\tau}_m^2} \quad (29)$$



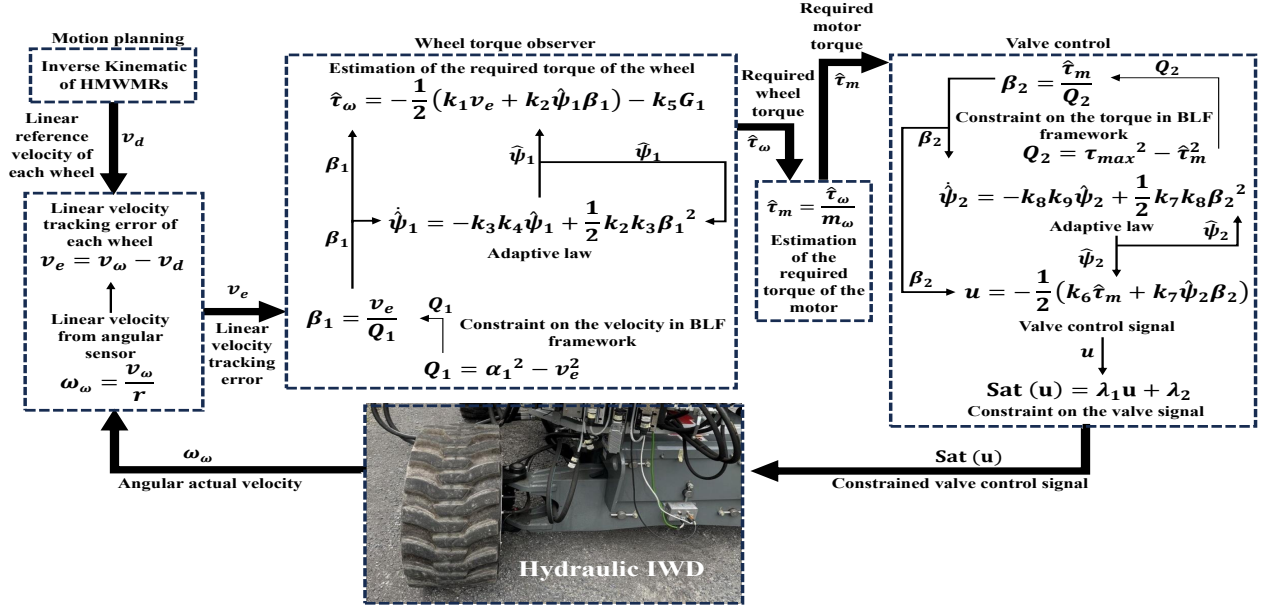


Fig. 4. Integration of the proposed RTOVC for each hydraulic-powered IWD-actuated wheel of the HWMR under uncertainties and safety constraints.

As observed in (29), if  $|\hat{\tau}_m(t_0)| < \hat{\tau}_{max}(t_0)$ , the motor torque must satisfy  $|\hat{\tau}_m| < \tau_{max}$ . Increasing  $\hat{\tau}_m^2$  and approaching to  $\tau_{max}^2$  leads to singularities in the system. For instance, in many programming platforms, execution may stop due to a warning, such as ‘Infinity or NaN value encountered,’ when the computed value exceeds the system’s numerical limits. It can prevent the issue of excessive motor torque generation, a common problem in velocity-based control systems, particularly during wheel slippage. Now, let us suggest the valve signal control, as follows:

$$u = -\frac{1}{2}(k_6 \hat{\tau}_m + k_7 \hat{\psi}_2 \beta_2) \quad (30)$$

$k_6$  is a positive constant. Since the entire hydraulic system model is assumed to be unknown, the proposed control in (30) does not include a modeling term  $G_2$  as seen in (24). Let us define the error of adaptation law, as:

$$\tilde{\psi}_2 = \hat{\psi}_2 - \psi_2^* \quad (31)$$

where  $\psi_2^*$  is an unknown positive constant. As  $a_2$  is a positive constant, let us introduce another logarithm-based BLF, as follows:

$$V_2 = \frac{1}{2a_2} \log\left(\frac{\tau_{max}^2}{Q_2}\right) + \frac{1}{2k_8} \tilde{\psi}_2^2 \quad (32)$$

where  $Q_2 = \tau_{max}^2 - \hat{\tau}_m^2$ . Similar to (29), according to the properties of logarithms in (32),  $Q_1$  cannot be zero or negative.

**Theorem 2:** Consider the logarithm-based BLF provided in (32). By applying the proposed valve control provided in (30) to the hydraulic IWD system provided in (15), under the constraints  $\text{Sat}(u) = \lambda_1 u + \lambda_2$  and  $|\hat{\tau}_m| < \tau_{max}$ , the system is uniformly exponentially stable into a region depending on the bound of uncertainties in the hydraulic system.

*Proof:* See **Appendix B**.

The integration of the individual RTOVC into each valve-based IWD of HMMRs is depicted in Fig. 4 and Algorithm 1. It is explained that after determining the reference linear velocity

for each wheel based on the inverse kinematics of the HWMR and upon receiving the actual velocity from the wheel’s velocity sensor, the RTOVC estimates the wheel torque necessary to align with the reference. Subsequently, the valve control signal generates sufficient motor torque to match the observed torque, while safety constraints are applied to the entire system.

#### Algorithm 1 Step-wise guidance of the RTOVC framework

**Input:** Measured velocity  $v_\omega$  and reference velocity  $v_d$ .

**Output:** Constrained valve control signal  $\text{Sat}(u)$ .

- 1 Obtain the velocity tracking error in each wheel:  $v_e = v_\omega - v_d$ ;
- 2 Calculate the velocity safety constraint notation:  $\beta_1 = \frac{v_e}{a_1^2 - v_e^2}$ ;
- 3 Estimate the first adaptive parameter:  $\dot{\hat{\psi}}_1 = -k_3 k_4 \hat{\psi}_1 + \frac{1}{2} k_2 k_3 \beta_1^2$ ;
- 4 Estimate the wheel torque:  $\hat{\tau}_\omega = -\frac{1}{2}(k_1 v_e + k_2 \hat{\psi}_1 \beta_1) - k_5 G_1$ ;
- 5 Calculate estimated hydraulic motor torque:  $\hat{\tau}_m = \frac{\tau_\omega}{m_\omega}$ ;
- 6 Calculate the torque safety constraint notation:  $\beta_2 = \frac{\hat{\tau}_m}{\tau_{max}^2 - \hat{\tau}_m^2}$ ;
- 7 Obtain control valve signal:  $u = -\frac{1}{2}(k_6 \hat{\tau}_m + k_7 \hat{\psi}_2 \beta_2)$ ;
- 8 Constrain the control valve signal:  $\text{Sat}(u) = \lambda_1 u + \lambda_2$ ;
- 9 Back to step 1.

#### 3.4. Stability of the proposed RTOVC framework for each hydraulic-powered IWD-actuated wheel of the HWMR

Now, consider the entire hydraulic-powered IWD-actuated wheel, which utilizes the proposed RTOVC framework, including the torque observer outlined in (24) and the valve control signal described in (30). Let us define a quadratic function, which is the sum of the quadratic functions (26) and (32), as follows:

$$\begin{aligned} \tilde{V} &= V_1 + V_2 \\ &= \frac{1}{2a_1} \log\left(\frac{a_1^2}{Q_1}\right) + \frac{1}{2a_2} \log\left(\frac{\tau_{max}^2}{Q_2}\right) + \frac{1}{2k_3} \tilde{\psi}_1^2 + \frac{1}{2k_8} \tilde{\psi}_2^2 \end{aligned} \quad (33)$$

**Theorem 3:** Consider the logarithm-based BLF provided in (33). By applying the proposed RTOVC framework, including the proposed torque observer outlined in (24) and the proposed valve control described in (30), to the whole hydraulic-powered IWD-actuated system including dynamics (2) and (15), under constraints provided in (19) and (10), wheel slippage and uncertainties, the actual linear velocity  $v_\omega$  of the wheel tracks the reference velocity  $v_d$  with uniformly exponentially stability into a stable region depending on the bound of uncertainties and intensity of wheel slippage on rough terrains.

*Proof:* See **Appendix C**.

### 3.5. Stability of the proposed RTOVC framework for the whole HWMR system actuated by four hydraulic-powered IWD-actuated wheel

For simplification, assume  $\alpha_2 = \tau_{max}$ . Now, let us define the following notation for  $i = 1, 2$ :

$$\Theta_i = \log \left( \frac{\alpha_i^2}{Q_i} \right) \quad (34)$$

If we assign the quadratic function provided in (33) to all four RTOVC-applied IWD-actuated wheels and sum them, we obtain the quadratic function of the whole RTOVC-applied IWD-actuated HWMR system, as:

$$\tilde{V} = \sum_{j=1}^4 \tilde{V}_j = \frac{1}{2} \sum_{j=1}^4 \frac{1}{a_{1,j}} \Theta_{1,j} + \frac{1}{a_{2,j}} \Theta_{2,j} + \frac{1}{k_{3,j}} \tilde{\psi}_{1,j}^2 + \frac{1}{k_{8,j}} \tilde{\psi}_{2,j}^2 \quad (35)$$

where  $j$  assigns the number of wheels for the quadratic function provided in (33). By differentiating (35) and similar to **Appendix C** and (72), we have:

$$\dot{\tilde{V}} \leq -\tilde{\Omega} \tilde{V} + \frac{1}{4} \sum_{j=1}^4 \sum_{i=1}^2 \rho_{2i-1,j}^{-1} m_{i,j}^2 + \tilde{\Omega} \quad (36)$$

where  $\tilde{\Omega} = \min\{\Omega_j \mid j = 1, \dots, 4\}$ .  $\Omega_j$  is the very  $\Omega$  provided in (73) for  $j$ th wheel. Similarly  $\tilde{\Omega} = \sum_{j=1}^4 \tilde{\Omega}_j$ .

**Theorem 4:** By applying the proposed RTOVC in all four hydraulic-powered IWD wheels of the HWMR, under wheel slippages, uncertainties, and safety-defined constraints in (19), the whole system of the HWMR is uniformly exponentially stable.

*Proof:* By performing the same mathematical manipulations as the equations provided from (74) to (88) in **Appendix C**, we obtain:

$$\Theta_{i,j} \leq \sqrt{\frac{2a_{i,j} \tilde{V}(t_0)}{1-Z}} e^{-\frac{1}{2}(t-t_0)} + \sqrt{\frac{2a_{i,j} \tilde{\Omega} \tilde{\Omega}^{-1}}{1-Z}} \quad (37)$$

Thus, based on [29], it is clear from (37),  $\Theta_{i,j}$  reaches a defined region  $\tilde{g}_0(\bar{\tau}_0)$  in uniformly exponential convergence, such that:

$$\tilde{g}_0(\bar{\tau}_0) := \left\{ \Theta_{i,j} \leq \bar{\tau}_0 := \sqrt{\frac{2\tilde{\Omega} \tilde{\Omega}^{-1}}{1-Z}} \right\} \quad (38)$$

## 4. Experimental Results and Analysis

### 4.1. Experimental Setup of the hydraulic-powered IWD-actuated HWMR

This section investigates the onboard implementation of the RTOVC applied to four independently high-bandwidth valve-based hydraulic-powered IWD-actuated wheels with the same diameter ( $r = 0.854$  m) of a 6,650-kg HWMR. The gear ratio of the reducer transmission for the wheel and in-wheel motor is  $m_\omega = 17.7$ .

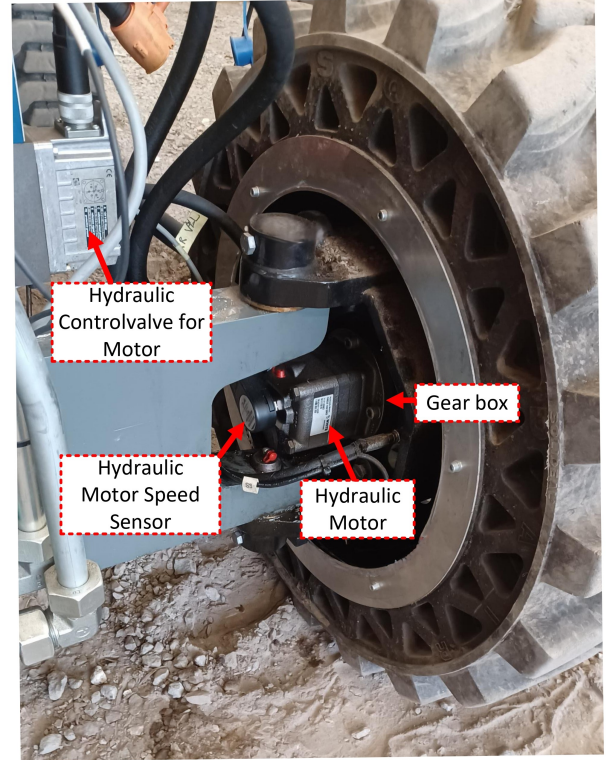


**Fig. 5.** Experimental setup of the studied hydraulic-powered IWD wheel.

**Table 1**

Instrumentation and hardware configuration of four hydraulic-powered IWD-actuated wheels of the studied HWMR system.

Component	Description
Kubota Diesel Engine	26.5kW @ 3000rpm
Bosch Rexroth Pump	63 l/min
Danfoss OMSS Motors	100 cm <sup>3</sup> /rev
Bosch Rexroth valves	40 l/min@ $\Delta p = 3.5$ MPa
IFM PA3521 transducers	sensor range: 25 MPa
Danfoss EMD Speed Sensor	0–2500 rpm
Beckhoff IPC CX2030	1000 Hz sample rate

The instrumentation and hardware of this setup are also provided in Fig. 5 and Table 1. In addition, the angular velocity of each wheel  $\omega_\omega$  was measured from an in-wheel electromagnetic speed sensor, which brings reliable navigation capabilities





**Fig. 6.** Experimental scenarios for the studied hydraulic-powered IWD-actuated HWMR are as follows: 1) snow-covered gravel terrain with soft soil and 2) ice-covered stony terrain with an approximate slope of 35 degrees.

to each hydraulic-powered IWD-actuated wheel control of the studied HWMR. The speed sensor detects the shaft speed and the direction of rotation, being mounted to the endcover of the Danfoss motor, and senses the speed from a magnet that is rotating inside the motor. The linear velocity of each wheel was calculated by  $v_\omega = r\omega_\omega$ . The communication between the case study and the computer is provided in Fig. 7.

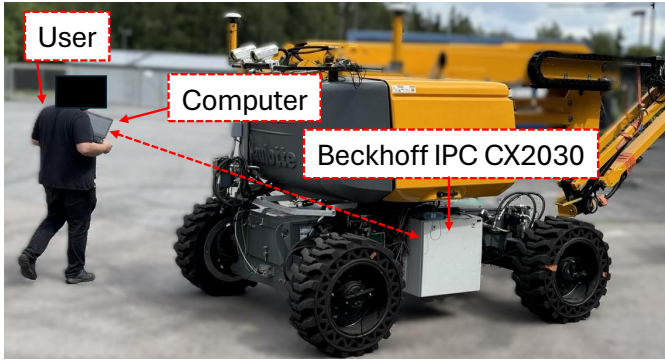


**Fig. 7.** Communication of the setup including sensory information and control commands.

As discussed, slippage and low friction between each wheel and the ground may introduce intense and unpredictable disturbances to the other wheels, challenging the platform's stability. Thus, when heavy-duty wheels rotate on rough or slippery terrain, the heavy-wight HWMR may lose control and stability during motion, potentially resulting in damage [33, 7]. To define realistic challenging scenarios for assessing the performance of RTOVC applied to four hydraulic-powered IWD-actuated wheels of the HWMR, the following tasks were considered:

- *Experiment 1:* The studied hydraulic-powered IWD-actuated HWMR moves at its maximum velocity ( $\approx 0.25$  m/s) on a snow-covered gravel terrain with soft soil and uneven surfaces. In this scenario, the IWDs are particularly susceptible to slippage due to the non-distributed heavy weight of the HWMR in the spot of the interaction between the wheel and the soft snowy surface. This scenario implicitly represents realistic off-road conditions that a hydraulic-powered IWD-actuated HWMR may experience.

- *Experiment 2:* The studied hydraulic-powered IWD-actuated HWMR moves at its maximum velocity on an ice-covered stony terrain with an approximate slope of 35 degrees. In this scenario, the increased gravitational resistance (during upward movement) and strain on the brakes (during backward movement) can cause the 6,650-kg IWD-actuated HWMR to skid or tip. In addition, the slippery icy surface complicates this situation.

Both scenarios are presented as image sequences (from left to right hand) in Fig. 6. Here, we abbreviate four hydraulic-powered IWD-actuated wheels of the HWMRs, as follows: front/left (FL), front/right (FR), rear/left (RL), and rear/right (RR) wheels. To investigate the capability of the motor torque observer (24) in the RTOVC framework, we did not have any information on the pressure or torque sensors of the wheels in the closed-loop control. The input to the RTOVC was the error between the in-wheel electromagnetic speed sensor-based actual linear velocities of the wheels (calculated from the motor velocities, gear ratios, and wheel radius) and the reference linear velocity generated by a joystick. The output consisted of four constrained control valve signals (see Fig. 8).

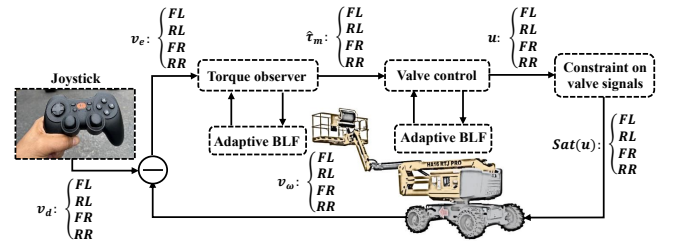


**Fig. 8.** The RTOVC-applied hydraulic-powered IWD-actuated HWMR in practice.

In addition, the safety-defined constraints in the RTOVC framework were defined, based on (19), in both experiments, as:

$$\begin{aligned} |v_\omega| &\leq \epsilon_1 = 0.4 \text{ m/s}, & |\tau_m| &< \tau_{max} = 290 \text{ N.m} \\ |\text{Sat}(u)| &\leq \bar{u} = u_{max} = 0.44, & |v_e| &< \alpha_1 = 0.4 - v_{max} \end{aligned} \quad (39)$$

$v_{max} = 0.25$  m/s is the maximum value of the reference wheel velocity ( $v_d$ ) generated by the joystick command, adjusted in

the joystick section built in the Beckhoff before each operational task. Furthermore, the maximum and minimum generated valve control signals were constrained as  $u_{max}$  and  $-u_{max}$ . The control parameters we used in this study are, as follows:  $k_1 = k_6 = 3$ ,  $k_2 = k_3 = k_4 = k_7 = k_8 = k_9 = 1$ , and  $k_5 = 100$ . Interestingly, except for  $k_1$  and  $k_6$ , the control performance of RTOVC was not visibly dependent on the other control parameters; being positive was sufficient for other constant parameters. A guide on parameter tuning of the proposed RTOVC is provided in **Appendix D**.

#### 4.2. Experiment 1: the hydraulic-powered IWD-actuated HWMR on the snow-covered gravel terrain with soft soil

The large-scale image of the IWD-actuated HWMR on the soft and rough terrain is shown in Fig.9.



**Fig. 9.** In Experiment 1, the performance of the studied HWMR was evaluated on a rough gravel terrain with a soft nature, covered by a layer of snow.

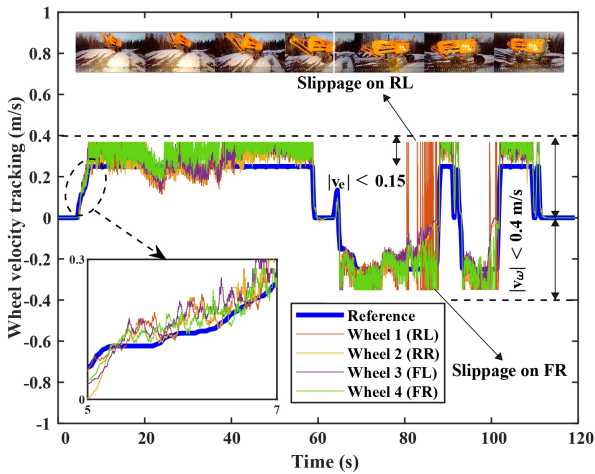


**Fig. 10.** Experiment 1 - Constrained wheels' velocity tracking error under RL and FR slippage.

During this execution, all wheels experienced slippages; in particular, the RL and FR wheels exhibited severe slippages during backward movement over a highly uneven spot with an extremely soft ground layer, occurring between 80 and 90 seconds after beginning the task. Despite this, the wheels' velocity tracking is shown in Fig. 10, indicating that all wheels, utilizing the RTOVC, perfectly tracked the joystick-generated velocity (depicted in blue). In addition, the safety-defined constraints on the actual velocity  $|v_{e}| < 0.4$  m/s and velocity tracking error  $|v_e| < 0.15$  m/s which were defined in (39) were also met. As observed, the actual velocities of the IWD-actuated wheels varied due to the uneven and non-smooth terrain, while still tracking the reference command. The large-scale image in Fig. 10 also illustrates the quick response of the RTOVC to changes in the velocities of the IWD-actuated wheels.

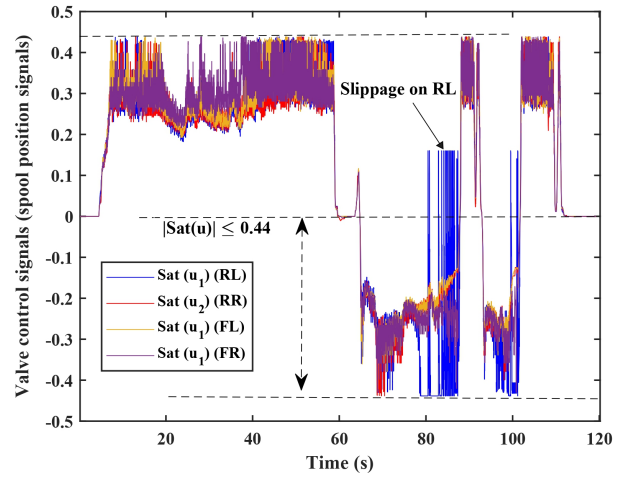


**Fig. 11.** Experiment 1 - Constrained valve control signals under RL and FR slippage.

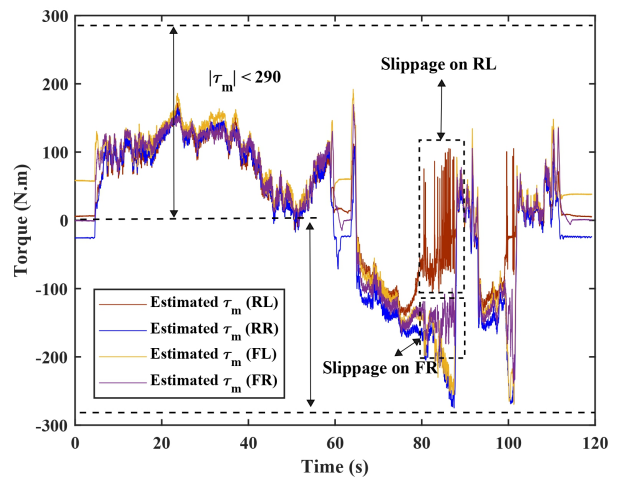


**Fig. 12.** Experiment 1 - Constrained and estimated motors' torques under RL and FR slippage.

The control valve signals generated by the RTOVC for this scenario are presented in Fig. 11. As observed during this scenario, the uneven and non-smooth terrain caused the control



signals to be generated excessively, leading to system instability and soil failure. However, the safety-defined constraints on all four valve signals as (39),  $|u| \leq 0.44$ , were adhered to. Similar to the constrained control valve signals and IWD velocities, the estimated motor torque never exceeded the safety-defined constraints,  $|\tau_m| \leq 290$ , as shown in Fig. 12, even under slippages. It is well-known that during slippage, the tracking velocity error increases, leading to the generation of excessive control command signals. This, in turn, causes the torque to be estimated excessively, further destabilizing the soil. However, as shown in Fig. 11, the control valve signals remained within their limits. This behavior is further corroborated by Fig. 12, which illustrates the estimated torques. All four hydraulic motor torques were maintained within the safe region. For instance, during the severe slippage of the RL wheel, the other motor torques tended to increase excessively to compensate for the disturbance caused by the RL wheel slippage but were effectively constrained within the safety limits, maintaining the whole system stable. Our detailed investigation revealed that, during this scenario, the IWD-actuated RR wheel achieved the best velocity tracking, with an average error of approximately 0.07 m/s. This performance surpassed the FL, FR, and RL wheels, which exhibited average errors of 0.08, 0.09, and 0.12 m/s, respectively. In addition, the highest torque effort was associated with the RR wheel, at 280 N·m, while the lowest was recorded for the RL wheel, at 175 N·m.

#### 4.3. Experiment 2: the hydraulic-powered IWD-actuated HWMR on the ice-covered stony terrain with an approximate slope of 35 degrees

The large-scale image of the IWD-actuated HWMR on the slippery and icy terrain is shown in Fig.13.



Fig. 13. In Experiment 2, the performance of the studied HWMR was evaluated on a slippery, icy, gravel terrain with an approximate slope of 35 degrees.

During this execution, all IWD-actuated wheels encountered a high slope and slippery surface. In particular, the FR wheel exhibited severe slippage during forward movement over the steepest section of the road, with a thick layer of ice, occurring between 100 and 115 seconds of the running task. Despite

this, the wheels' velocity tracking is shown in Fig. 14, indicating that all wheels, utilizing the RTOVC, perfectly tracked the joystick-generated velocity (depicted in blue). In addition, similar to Experiment 1, the safety-defined constraints on the actual velocity  $|v_\omega| < 0.4$  m/s and velocity tracking error  $|v_e| < 0.15$  m/s which were defined in (39) were met.

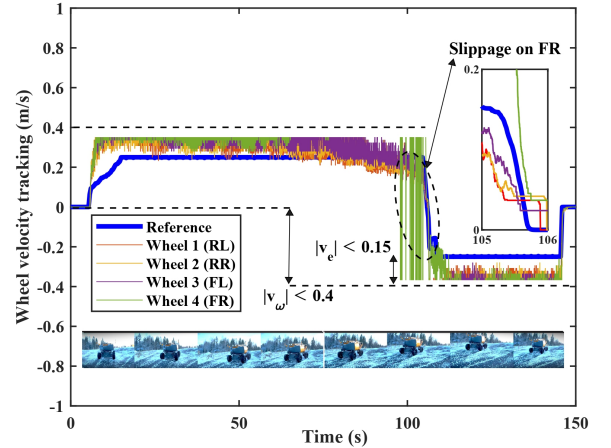


Fig. 14. Experiment 2 - Constrained wheels' velocity tracking error under FR slippage.

As observed in Fig. 14, the absolute actual velocities of the IWD-actuated wheels were more than the velocity command due to the increased gravitational forces. The large-scale image in Fig. 14 further illustrates the quick response of the RTOVC and its capability to track changes in the velocities of the IWD-actuated wheels during the slippage of the FR wheel.

The control valve signals generated by the RTOVC for this scenario are presented in Fig. 15. As observed during this scenario, the high slope and slippery terrain caused the control signals to be generated excessively, leading to system instability. However, the safety-defined constraints on all four valve signals as (39),  $|u| \leq 0.44$ , were adhered to.

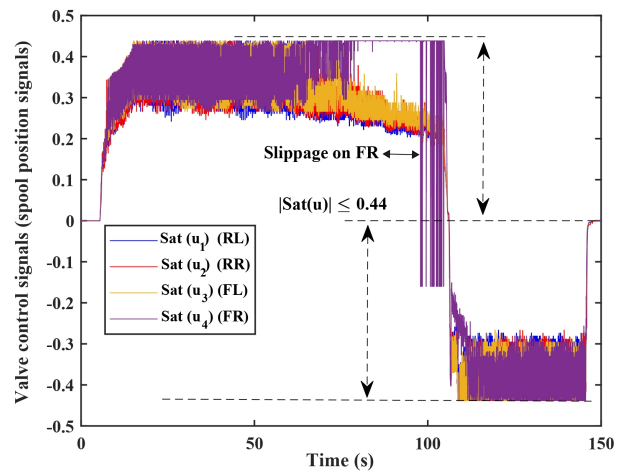
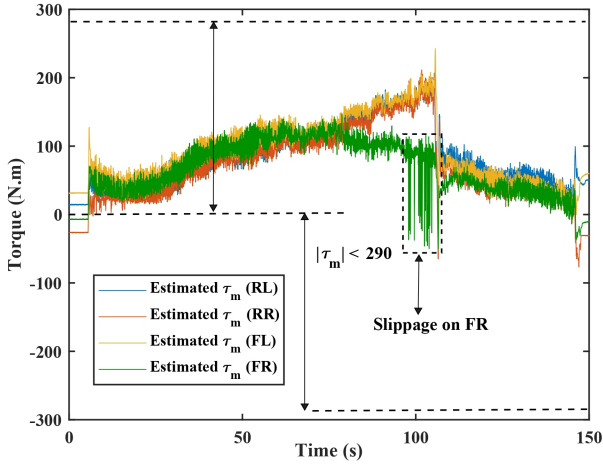


Fig. 15. Experiment 2 - Constrained valve control signals under FR slippage.

Similar to the constrained control valve signals and IWD velocities, the estimated motor torque never exceeded the safety-

defined constraints,  $|\tau_m| \leq 290$ , as shown in Fig. 16, even under slippage.



**Fig. 16.** Experiment 2 - Constrained and estimated motors' torques under FR slippage.

As mentioned earlier in Experiment 1, during slippage, the tracking velocity error increases, leading to the generation of excessive control command signals. This, in turn, causes the torque to be generated excessively, further destabilizing the system. However, as shown in Fig. 15, the control valve signals remained within their limits. This behavior is further corroborated by Fig. 16, which illustrates the estimated torques. All four hydraulic motor torques were maintained within the safe region. For instance, during the severe slippage of the FR wheel, the other motor torques tended to increase excessively to compensate for the disturbance caused by the FR wheel slippage but were effectively constrained within the safety limits, maintaining the whole system stable. Our detailed investigation revealed that, during this scenario, the IWD-actuated RR wheel achieved the best velocity tracking, with an average error of approximately 0.08 m/s. This performance surpassed the FL, RL, and FR wheels, which exhibited average errors of 0.09, 0.09, and 0.13 m/s, respectively. In addition, the highest torque effort was associated with the FL wheel, at 240 N·m, while the lowest was recorded for the RL wheel, at 100 N·m.

All two experiments demonstrated the robustness of the RTOVC framework under challenging slippery terrains. Table 2 summarizes the performances of the RTOVC, a model-free robust backstepping-based adaptive control (BAC), as proposed in [34], and a model-based robust decentralized-valve-structure control (DVSC), as proposed in [35] for the studied IWD-actuated HWMR in the same condition. To ensure a fairer comparison, the selected tracking criteria—velocity error and torque efforts—were based on the average velocity error (m/s) and the maximum motor efforts (N·m) during movement. Note that unlike the RTOVC, which uses a torque observer, the implementation of the BAC and DVSC schemes utilized torque feedback via the HWMR's pressure sensors without the safety-defined constraints, resorting to the emergency push button when necessary. In addition to uniformly exponen-

tial stability, torque observation, and safety-defined constraints, the tracking performances detailed in the table indicate an improvement in controlling the studied four hydraulic-powered IWD-actuated HWMR by employing the RTOVC framework. We also employed the proportional–integral–derivative (PID) controller for the case study, however, we were unable to control the HWMR effectively using the PID controller because it may be adequate only for systems primarily characterized by second-order dynamics [36], while the higher-order-dynamic hydraulic-powered IWD-actuated HWMR exposed severe disturbances due to slipping terrains and uncertainties in hydraulic drive systems.

**Table 2**

Performance of the HWMR wheels implemented by the RTOVC, DVSC [35], and BAC [34] in two experiments under slippages.

Exp.	Wheel	criteria	RTOVC	DVSC [35]	BAC [34]
1	RL	Vel. error / Torque	0.12/175	0.18/220	0.25/300
	RR	Vel. error / Torque	0.07/280	0.12/300	0.10/310
	FL	Vel. error / Torque	0.08/275	0.14/295	0.14/320
	FR	Vel. error / Torque	0.09/250	0.11/290	0.18/290
2	RL	Vel. error / Torque	0.09/100	0.09/125	0.15/145
	RR	Vel. error / Torque	0.08/200	0.16/235	0.21/240
	FL	Vel. error / Torque	0.09/240	0.12/280	0.30/320
	FR	Vel. error / Torque	0.13/125	0.19/155	0.23/205

## 5. Conclusion & future work

To address the vital requirement for advancements in designing a strongly stability-guaranteed, safe, and robust control system for hydraulic-powered IWD-actuated HWMR systems in uncertain and time-varying operating conditions, this paper proposed the RTOVC within a logarithmic BLF framework. It decreased the closed-loop dependency associated with fault-prone sensors by estimating the required torque of each hydraulic-powered IWD-actuated wheel of the distributed HWMR system using a novel robust adaptive BLF-based observer to track the desired velocity. In addition, another robust adaptive BLF-based control was employed for the hydraulic system to manage the valve control signals, generating the same estimated torque for each wheel. The RTOVC framework including the proposed robust torque observer and robust valve control reduces the risk of system faults by safely constraining key input-output signals—such as the actual velocities, tracking errors, motor/wheel torques, and control valve signals of hydraulic-powered IWD-actuated wheels within logarithmic BLFs. Our study found that a 6,500-kg HWMR employing four RTOVC-applied hydraulic-powered IWD-actuated wheels achieved strong robustness and stability of the whole system, even in the presence of safety-defined constraints and disturbances, such as severe wheel slippage on rough terrains. This work may pave the way for potential future expansions into electrically-driven HWMRs by viewing the IWD mechanism as electrical and voltage-based with torque/current estimation rather than hydraulic and valve-based with torque/pressure estimation.

## CRedit authorship contribution statement

**Mehdi Heydari Shahna:** Writing - original draft, Validation, Methodology, Investigation, Formal analysis, Software, Conceptualization.

**Pauli Mustalahti:** Validation, Resources, Data curation, Investigation.

**Jouni Mattila:** Writing - review & editing, Resources, Supervision, Funding acquisition.

## Declaration of competing interest

The authors declare that they have no known competing financial interests or personal relationships that could have appeared to influence the work reported in this paper.

## Acknowledgement

This work was supported by the Business Finland Partnership Project, ‘Future All-Electric Rough Terrain Autonomous Mobile Manipulators’ under Grant No. 2334/31/2022.

## Appendix A. Stability analysis of the proposed torque estimation for wheel motion dynamics under slippage and uncertainties in the presence of safety-defined constraints

*Proof of Theorem 1:* As  $\psi_1^*$  is positive constant, let us use (25) and (22) to provide:

$$\dot{\tilde{\psi}}_1 = -k_3 k_4 \tilde{\psi}_1 + \frac{1}{2} k_2 k_3 \beta_1^2 - k_3 k_4 \psi_1^* \quad (40)$$

Recall that  $\beta_1 = \frac{v_e}{Q_1}$ . Therefore, by taking the derivative of (26) considering (18):

$$\dot{V}_1 = \beta_1 \tau_\omega + \frac{1}{a_1} \beta_1 F_1^* + \frac{1}{a_1} \beta_1 G_1 + \frac{1}{a_1} \beta_1 D_1 + k_3^{-1} \tilde{\psi}_1 \dot{\tilde{\psi}}_1 \quad (41)$$

To be control design meaningful, functions due to uncertainties and external disturbances  $F_1$ , and  $D_1$  must be bounded. Let us assume  $\dot{\omega}_d$  exists. Thus, based on (18), we can assume  $F_1^*$  is also bounded. Based on these assumptions, let us introduce  $\mu_1$  and  $D_1^* \in \mathbb{R}^+$  as unknown positive constants, and  $m_1 : \mathbb{R} \rightarrow \mathbb{R}^+$  as a continuously bounded function with strictly positive values. They assign the upper bound of  $F_1^*$  and  $D_1$ , as:

$$\|F_1^*\| \leq \mu_1 m_1, \quad \|D_1\| \leq D_1^* \quad (42)$$

Then, from (41) and (42):

$$\dot{V}_1 \leq \beta_1 \tau_\omega + \frac{1}{a_1} \mu_1 m_1 |\beta_1| + \frac{1}{a_1} \beta_1 G_1 + \frac{1}{a_1} D_1^* |\beta_1| + k_3^{-1} \tilde{\psi}_1 \dot{\tilde{\psi}}_1 \quad (43)$$

Now, by utilizing the proposed torque estimation  $\hat{\tau}_\omega$  provided in (24) instead of  $\tau_\omega$  in (43), we have:

$$\begin{aligned} \dot{V}_1 \leq & -\frac{1}{2} \beta_1 k_1 v_e - \frac{1}{2} k_2 \hat{\psi}_1 \beta_1^2 - k_5 \beta_1 G_1 + \frac{1}{a_1} \mu_1 m_1 |\beta_1| \\ & + \frac{1}{a_1} \beta_1 G_1 + \frac{1}{a_1} D_1^* |\beta_1| + k_3^{-1} \tilde{\psi}_1 \dot{\tilde{\psi}}_1 \end{aligned} \quad (44)$$

Consider that  $\rho_1$  and  $\rho_2$  are any positive constants. Let us choose  $k_5$  large enough to satisfy  $k_5 \geq a_1^{-1}$ . Using algebraic manipulations and Young’s inequality, we can have:

$$\begin{aligned} \dot{V}_1 \leq & -\frac{1}{2} \beta_1 k_1 v_e - \frac{1}{2} k_2 \hat{\psi}_1 \beta_1^2 + \frac{1}{4} \rho_1^{-1} m_1^2 + \frac{1}{4} \rho_2^{-1} + \rho_2 \left(\frac{1}{a_1}\right)^2 D_1^{*2} \beta_1^2 \\ & + \rho_1 \left(\frac{1}{a_1}\right)^2 \mu_1^2 \beta_1^2 + k_3^{-1} \tilde{\psi}_1 \dot{\tilde{\psi}}_1 \end{aligned} \quad (45)$$

Let us introduce unknown positive constant  $\psi_1^*$ , as:

$$\psi_1^* = \frac{2}{k_2} \left( \rho_2 \frac{1}{a_1^2} D_1^{*2} + \rho_1 \frac{1}{a_1^2} \mu_1^2 \right) \quad (46)$$

Thus, from (45) and (46), we obtain:

$$\begin{aligned} \dot{V}_1 \leq & -\frac{1}{2} \beta_1 k_1 \omega_e - \frac{1}{2} k_2 \hat{\psi}_1 \beta_1^2 + \frac{1}{4} \rho_1^{-1} m_1^2 + \frac{1}{2} k_2 \psi_1^* \beta_1^2 + \frac{1}{4} \rho_2^{-1} \\ & + k_3^{-1} \tilde{\psi}_1 \dot{\tilde{\psi}}_1 \end{aligned} \quad (47)$$

Inserting (40) into (47), we obtain:

$$\begin{aligned} \dot{V}_1 \leq & -\frac{1}{2} \beta_1 k_1 v_e - \frac{1}{2} k_2 (\hat{\psi}_1 - \psi_1^*) \beta_1^2 + \frac{1}{4} \rho_1^{-1} m_1^2 + \frac{1}{4} \rho_2^{-1} - k_4 \tilde{\psi}_1^2 \\ & + \frac{1}{2} k_2 \tilde{\psi}_1 \beta_1^2 - k_4 \psi_1^* \tilde{\psi}_1 \end{aligned} \quad (48)$$

Recall that  $\beta_1 = \frac{v_e}{Q_1}$ . Thus:

$$\begin{aligned} \dot{V}_1 \leq & -\frac{1}{2} k_1 \frac{v_e^2}{Q_1} + \frac{1}{4} \rho_1^{-1} m_1^2 + \frac{1}{4} \rho_2^{-1} - \frac{1}{2} k_4 \tilde{\psi}_1^2 - \frac{1}{2} k_4 (\hat{\psi}_1 - \psi_1^*)^2 \\ & - k_4 \psi_1^* (\hat{\psi}_1 - \psi_1^*) \end{aligned} \quad (49)$$

Note that the initial condition of (22) must be  $\hat{\psi}_1(t_0) > 0$ , guaranteeing  $\hat{\psi}_1(t) > 0$  for any  $t \geq t_0$ . Thus, by knowing  $\hat{\psi}_1$  is always positive, we can Simplify (49), as:

$$\dot{V}_1 \leq -\frac{1}{2} k_1 \frac{v_e^2}{Q_1} + \frac{1}{4} \rho_1^{-1} m_1^2 + \frac{1}{4} \rho_2^{-1} - \frac{1}{2} k_4 \tilde{\psi}_1^2 + \frac{1}{2} k_4 \psi_1^{*2} \quad (50)$$

According to [37] and knowing  $Q_1 = \alpha_1^2 - v_e^2$ , if  $|v_e| < \alpha_1$ , we have:

$$\log\left(\frac{\alpha_1^2}{Q_1}\right) < \frac{v_e^2}{Q_1} \quad (51)$$

Thus, from (50) and (51), we have:

$$\dot{V}_1 \leq -\frac{1}{2} k_1 \log\left(\frac{\alpha_1^2}{Q_1}\right) + \frac{1}{4} \rho_1^{-1} m_1^2 + \frac{1}{4} \rho_2^{-1} - \frac{1}{2} k_4 \tilde{\psi}_1^2 + \frac{1}{2} k_4 \psi_1^{*2} \quad (52)$$

or simply from (52), we can say:

$$\dot{V}_1 \leq -\Omega_{11} V_1 + \frac{1}{4} \rho_1^{-1} m_1^2 + \Omega_{12} \quad (53)$$

where

$$\Omega_{11} = \min\left[ a_1 k_1, \quad k_3 k_4 \right], \quad \Omega_{12} = \frac{1}{4} \rho_2^{-1} + \frac{1}{2} k_4 \psi_1^{*2} \quad (54)$$

Thus, based on [31] and [38], by applying the proposed torque estimation to the IWD, the error of linear velocity, under the constraint  $|v_e| < \alpha_1$ , in the presence of wheel slippage uniformly exponentially converges into the region. the radius of which depends on  $\psi_1^*$  [30].  $\psi_1^*$  is based on the bound of uncertainties  $\mu_1$  and external disturbances  $D_1^*$  due to the modeling error and wheel slip (see (46)).



## Appendix B. Stability analysis of the proposed robust valve control for the hydraulic-powered IWD system under system uncertainties in the presence of safety-defined constraints

*Proof of Theorem 2:* As  $\psi_2^*$  is an unknown positive constant, let us use (28) and (31):

$$\dot{\tilde{\psi}}_2 = -k_8 k_9 \tilde{\psi}_2 + \frac{1}{2} k_7 k_8 \beta_2^2 - k_8 k_9 \psi_2^* \quad (55)$$

Recall that  $\beta_2 = \frac{\hat{\tau}_m}{Q_2}$ . Thus, by taking the derivative of (32) and considering (15):

$$\dot{V}_2 = \beta_2 u + \frac{1}{a_2} \beta_2 F_2 + \frac{1}{a_2} \beta_2 D_2 + k_8^{-1} \tilde{\psi}_2 \dot{\tilde{\psi}}_2 \quad (56)$$

To be control design meaningful, functions due to uncertainties and external disturbances  $F_2$ , and  $D_2$  must be bounded. Based on these assumptions, let us introduce  $\mu_2$  and  $D_2^* \in \mathbb{R}^+$  as unknown positive constants, and  $m_2 : \mathbb{R} \rightarrow \mathbb{R}^+$  as a continuously bounded function with strictly positive values. They assign the upper bound of  $F_2$  and  $D_2$ , as:

$$\|F_2\| \leq \mu_2 m_2, \quad \|D_2\| \leq D_2^* \quad (57)$$

Then, from (57) and (56):

$$\dot{V}_2 \leq \beta_2 u + \frac{1}{a_2} \mu_2 m_2 |\beta_2| + \frac{1}{a_2} D_2^* |\beta_2| + k_8^{-1} \tilde{\psi}_2 \dot{\tilde{\psi}}_2 \quad (58)$$

Now, by inserting the proposed valve control signal provided in (30) into (58), we have:

$$\begin{aligned} \dot{V}_2 \leq & -\frac{1}{2} \beta_2 k_6 \hat{\tau}_m - \frac{1}{2} k_6 \hat{\psi}_2 \beta_2^2 + \frac{1}{a_2} \mu_2 m_2 |\beta_2| + \frac{1}{a_2} D_2^* |\beta_2| \\ & + k_8^{-1} \tilde{\psi}_2 \dot{\tilde{\psi}}_2 \end{aligned} \quad (59)$$

Consider that  $\rho_3$  and  $\rho_4$  are any positive constants. Using algebraic manipulations and Young's inequality, we can have:

$$\begin{aligned} \dot{V}_2 \leq & -\frac{1}{2} \beta_2 k_6 \hat{\tau}_m - \frac{1}{2} k_7 \hat{\psi}_2 \beta_2^2 + \frac{1}{4} \rho_3^{-1} m_2^2 + \frac{1}{4} \rho_4^{-1} + \rho_4 \left(\frac{1}{a_2}\right)^2 D_2^{*2} \beta_2^2 \\ & + \rho_3 \left(\frac{1}{a_2}\right)^2 \mu_2^2 \beta_2^2 + k_8^{-1} \tilde{\psi}_2 \dot{\tilde{\psi}}_2 \end{aligned} \quad (60)$$

Let us introduce unknown positive constant  $\psi_2^*$ , as:

$$\psi_2^* = \frac{2}{k_7} \left( \rho_4 \frac{1}{a_2} D_2^{*2} + \rho_3 \frac{1}{a_2} \mu_2^2 \right) \quad (61)$$

Thus, from (60) and (61), we obtain:

$$\begin{aligned} \dot{V}_2 \leq & -\frac{1}{2} \beta_2 k_6 \hat{\tau}_m - \frac{1}{2} k_7 (\hat{\psi}_2 - \psi_2^*) \beta_2^2 + \frac{1}{4} \rho_3^{-1} m_2^2 + \frac{1}{2} k_7 \psi_2^* \beta_2^2 + \frac{1}{4} \rho_4^{-1} \\ & + k_8^{-1} \tilde{\psi}_2 \dot{\tilde{\psi}}_2 \end{aligned} \quad (62)$$

Inserting (55) into (62), we obtain:

$$\begin{aligned} \dot{V}_2 \leq & -\frac{1}{2} \beta_2 k_6 \hat{\tau}_m - \frac{1}{2} k_7 (\hat{\psi}_2 - \psi_2^*) \beta_2^2 + \frac{1}{4} \rho_3^{-1} m_2^2 + \frac{1}{4} \rho_4^{-1} - k_9 \tilde{\psi}_2^2 \\ & + \frac{1}{2} k_7 \tilde{\psi}_2 \beta_2^2 - k_9 \psi_2^* \tilde{\psi}_2 \end{aligned} \quad (63)$$

Recall that  $\beta_2 = \frac{\hat{\tau}_m}{Q_2}$ . Thus:

$$\begin{aligned} \dot{V}_2 \leq & -\frac{1}{2} k_2 \frac{\hat{\tau}_m^2}{Q_2} + \frac{1}{4} \rho_3^{-1} m_2^2 + \frac{1}{4} \rho_4^{-1} - \frac{1}{2} k_9 \tilde{\psi}_2^2 - \frac{1}{2} k_9 (\hat{\psi}_2 - \psi_2^*)^2 \\ & - k_9 \psi_2^* (\hat{\psi}_2 - \psi_2^*) \end{aligned} \quad (64)$$

Note that the initial condition of (28) must be  $\hat{\psi}_2(t_0) > 0$ , guaranteeing  $\hat{\psi}_2(t) > 0$  for any  $t \geq t_0$ . Thus, by knowing  $\hat{\psi}_2$  is always positive, we can Simplify (64), as:

$$\dot{V}_2 \leq -\frac{1}{2} k_6 \frac{\hat{\tau}_m^2}{Q_2} + \frac{1}{4} \rho_3^{-1} m_2^2 + \frac{1}{4} \rho_4^{-1} - \frac{1}{2} k_9 \tilde{\psi}_2^2 + \frac{1}{2} k_9 \psi_2^{*2} \quad (65)$$

According to [37] and knowing  $Q_2 = \tau_{max}^2 - \hat{\tau}_m^2$ , if  $|\hat{\tau}_m| < \tau_{max}$ , we have:

$$\log\left(\frac{\tau_{max}^2}{Q_2}\right) < \frac{\hat{\tau}_m^2}{Q_2} \quad (66)$$

Thus, from (66) and (65), we have:

$$\dot{V}_2 \leq -\frac{1}{2} k_6 \log\left(\frac{\tau_{max}^2}{Q_2}\right) + \frac{1}{4} \rho_3^{-1} m_2^2 + \frac{1}{4} \rho_3^{-1} - \frac{1}{2} k_9 \tilde{\psi}_2^2 + \frac{1}{2} k_9 \psi_2^{*2} \quad (67)$$

or simply from (67), we can say:

$$\dot{V}_2 \leq -\Omega_{21} V_2 + \frac{1}{4} \rho_3^{-1} m_2^2 + \Omega_{22} \quad (68)$$

where

$$\Omega_{21} = \min\left[ a_2 k_6, \quad k_8 k_9 \right], \quad \Omega_{22} = \frac{1}{4} \rho_4^{-1} + \frac{1}{2} k_9 \psi_2^{*2} \quad (69)$$

Thus, based on [31] and [38], by applying the proposed valve control signal  $u$ , the hydraulic system, under the constraint  $|\hat{\tau}_m| < \tau_{max}$ , in the presence of uncertainties, is uniformly exponential stable into the region. the radius of which depends on  $\psi_2^*$  [30].  $\psi_2^*$  is based on the bound of uncertainties  $\mu_2$  and external disturbances  $D_2^*$  due to hydraulic uncertainties (see (61)).

## Appendix C. Stability analysis of the proposed RTOVC framework for each hydraulic-powered IWD-actuated wheel of the HWMR under wheel slippage and system uncertainties in the presence of safety-defined constraints

For simplification, assume  $\alpha_2 = \tau_{max}$ . Now, let us define the following notation for  $i = 1, 2$ :

$$\Theta_i = \log\left(\frac{\alpha_i^2}{Q_i}\right) \quad (70)$$

Based on (33), we have:

$$\bar{V} = \frac{1}{2a_1} \Theta_1 + \frac{1}{2a_2} \Theta_2 + \frac{1}{2k_3} \tilde{\psi}_1^2 + \frac{1}{2k_8} \tilde{\psi}_2^2 \quad (71)$$

The derivative of (71), based on (53) and (68), can be expressed, as:

$$\dot{\bar{V}} = \dot{V}_1 + \dot{V}_2 \leq -\Omega \bar{V} + \frac{1}{4} \sum_{i=1}^2 \rho_{2i-1}^{-1} m_i^2 + \bar{\Omega} \quad (72)$$

where

$$\begin{aligned} \Omega &= \min\{\Omega_{11}, \Omega_{21}\} = \min\{a_1, k_1, a_2 k_6, k_3 k_4, k_8 k_9\} \\ \bar{\Omega} &= \Omega_{12} + \Omega_{22} = \frac{1}{4} \rho_2^{-1} + \frac{1}{2} k_4 \psi_1^{*2} + \frac{1}{4} \rho_4^{-1} + \frac{1}{2} k_9 \psi_2^{*2} \end{aligned} \quad (73)$$

Therefore:

$$\bar{V} \leq \bar{V}(t_0) e^{-\{\Omega(t-t_0)\}} + \bar{\Omega} \Omega^{-1} + \frac{1}{4} \sum_{i=1}^2 \rho_{2i-1}^{-1} \int_{t_0}^t e^{-\Omega(t-T)} m_i^2 dT \quad (74)$$

From (71) and (70), we can say for  $i = 1, 2$ :

$$\Theta_i^2 \leq 2a_i \bar{V}(t_0) e^{-\{\Omega(t-t_0)\}} + 2a_i \bar{\Omega} \Omega^{-1} + \frac{1}{2} a_i \sum_{i=1}^2 \rho_{2i-1}^{-1} \int_{t_0}^t e^{-\Omega(t-T)} r_i^2 dT \quad (75)$$

A continuous operator can be suggested as:

$$Z(\iota) = \frac{0.5}{\Omega - \iota} > 0 \quad (76)$$

where  $\iota \in [0, \Omega)$ . Note  $Z(0) = \frac{1}{2\Omega} \leq Z(\iota)$ . We are able to find a sufficient small parameter  $\bar{\iota} \in \iota$  that satisfies the following condition:

$$0 < \bar{Z} = Z(\bar{\iota}) = \frac{0.5}{\Omega - \bar{\iota}} < 1 \quad (77)$$

By multiplying  $e^{\bar{\iota}(t-t_0)}$ , we reach:

$$\Theta_i e^{\bar{\iota}(t-t_0)} \leq 2a_i \bar{V}(t_0) e^{-(\Omega-\bar{\iota})(t-t_0)} + 2a_i \bar{\Omega} \Omega^{-1} e^{\bar{\iota}(t-t_0)} + \frac{1}{2} a_i \sum_{i=1}^2 \rho_{2i-1}^{-1} \int_{t_0}^t e^{-\Omega(t-T)+\bar{\iota}(t-t_0)} m_i^2 dT \quad (78)$$

We can omit the reducing element that existed on the right-hand side, as:

$$\Theta_i e^{\bar{\iota}(t-t_0)} \leq 2a_i \bar{V}(t_0) + 2a_i \bar{\Omega} \Omega^{-1} e^{\bar{\iota}(t-t_0)} + \frac{1}{2} a_i \sum_{i=1}^2 \rho_{2i-1}^{-1} \int_{t_0}^t e^{-\Omega(t-T)+\bar{\iota}(t-t_0)} m_i^2 dT \quad (79)$$

Using this approach, we can describe functions  $E_0$  and  $E_1$ , which are continuous:

$$E_0 = \Theta_i^2 e^{\bar{\iota}(w-t_0)}$$

$$E_1 = \sup_{w \in [t_0, t]} \left[ \sum_{i=1}^2 \rho_{2i-1}^{-1} (m_i^2) e^{\bar{\iota}(w-t_0)} \right] \quad (80)$$

Next, by considering (79) and (80), and knowing  $\bar{\iota} \geq 0$ , we obtain:

$$E_0 \leq 2a_i \bar{V}(t_0) + 2a_i \bar{\Omega} \Omega^{-1} + \frac{0.5a_i}{\Omega - \bar{\iota}} E_1 \quad (81)$$

By defining  $\bar{E} = \max(E_0, E_1)$ , we can have:

$$E_0 \leq 2a_i \bar{V}(t_0) + 2a_i \bar{\Omega} \Omega^{-1} e^{\bar{\iota}(t-t_0)} + \bar{Z} a_i \bar{E} \quad (82)$$

It is always possible to ensure the existence of  $\bar{\iota}$  and  $\iota^*$ , where  $\bar{Z}$  sufficiently small in (77) and  $\Omega > \iota^* > \bar{\iota}$ , to satisfy the following condition [31]:

$$\bar{Z} = Z(\iota^*) > \bar{Z}, \quad 0 < \bar{Z} < 1, \quad \bar{Z} a_i \bar{E} \leq \bar{Z} E_0 \quad (83)$$

Inserting (83) into (82), we arrive at:

$$E_0 \leq 2a_i \bar{V}(t_0) + 2a_i \bar{\Omega} \Omega^{-1} e^{\bar{\iota}(t-t_0)} + \bar{Z} E_0 \quad (84)$$

Afterward, we have:

$$E_0 \leq \frac{2a_i \bar{V}(t_0) + 2a_i \bar{\Omega} \Omega^{-1} e^{\bar{\iota}(t-t_0)}}{1 - \bar{Z}} \quad (85)$$

Concerning the definition of  $E_0$  in (80), we achieve:

$$\Theta_i^2 \leq \frac{2a_i \bar{V}(t_0) e^{-\bar{\iota}(t-t_0)} + 2a_i \bar{\Omega} \Omega^{-1}}{1 - \bar{Z}} \quad (86)$$

Based on Minkowski's inequality, we reach:

$$\Theta_i \leq \sqrt{\frac{2a_i \bar{V}(t_0)}{1 - \bar{Z}}} e^{-\frac{\bar{\iota}}{2}(t-t_0)} + \sqrt{\frac{2a_i \bar{\Omega} \Omega^{-1}}{1 - \bar{Z}}} \quad (87)$$

Thus, based on **Definition 1**, [29], it is clear from (87),  $\Theta_i$  reaches a defined region  $g_0(\tau_0)$  in uniformly exponential convergence, such that:

$$g_0(\tau_0) := \left\{ \Theta_i \leq \bar{\tau}_0 := \sqrt{\frac{2\bar{\Omega} \Omega^{-1}}{1 - \bar{Z}}} \right\} \quad (88)$$

#### Appendix D. A guide on parameter tuning of the proposed RTOVC including the proposed torque observer and robust valve control

For each hydraulic-powered IWD-actuated wheel, the following steps are required individually:

- Step (1) Define safety constraints for the velocity tracking error of the wheel  $\alpha_1$ , the actual velocity of the wheel  $\epsilon_1$ , the hydraulic motor torque  $\tau_{max}$ , and valve control signal  $u_{max}$ .

- Step (2) As we assumed in (44) and (45),  $k_5 \geq a_1^{-1} = \frac{J_{\omega}}{r}$ . Thus,  $k_5$  is chosen large enough.

- Step (3) For each wheel, separately,  $k_1$  and  $k_6$  are carefully selected, considering the trade-off between robustness and the tracking system's responsiveness. Increasing these values will enhance the wheel system's robustness against disturbances, wheel slippage, and the intensity of uncertainties in the hydraulic-powered IWD while reducing tracking accuracy. As the slippage potential of the field and uncertainties are unknown, the chosen  $k_1$  and  $k_6$  are adjusted by increasing them slightly until the actual velocity of the hydraulic IWD-actuated wheel perfectly tracks the desired velocity, meaning that they compensate for the disturbance and uncertainties.

- Step (4) When the tracking error converges to zero with the parameters chosen in Steps 1 and 2, adjust the other parameters ( $k_2, k_3, k_4, k_7, k_8$ , and  $k_9$ ) as needed. Interestingly, changing these parameters does not visibly affect the overall control performance. However, based on our experience, their adjustment slightly influences the convergence rate, reducing the required step times for the RTOVC.

- Step (5) Go back to Step (2) if the tracking performance does not reach a desired level.

#### References

- [1] S. Yamada, T. Beauvain, H. Fujimoto, T. Kanou, E. Katsuyama, Active model-based suppression of secondary ride for electric vehicles with in-wheel motors, IEEE/ASME Transactions on Mechatronics 27 (6) (2022) 5637–5646.
- [2] X. Shao, F. Naghdy, H. Du, Reliable fuzzy h control for active suspension of in-wheel motor driven electric vehicles with dynamic damping, Mechanical Systems and Signal Processing 87 (2017) 365–383.

- [3] M. Ghazali, Path-following and tire loss investigation of a front in-wheel-drive electric vehicle with off-centre cg, *Mechanism and Machine Theory* 189 (2023) 105422.
- [4] F. R. von Glehn, B. H. P. Gonçalves, M. G. F. Neto, J. P. da Silva Fonseca, Telematics and machine learning system for estimating the load condition of a heavy-duty vehicle, *Procedia Computer Science* 232 (2024) 2616–2625.
- [5] A. Kobelski, P. Osinenko, S. Streif, Experimental verification of an on-line traction parameter identification method, *Control Engineering Practice* 113 (2021) 104837.
- [6] D. Fassbender, V. Zakharov, T. Minav, Utilization of electric prime movers in hydraulic heavy-duty-mobile-machine implement systems, *Automation in Construction* 132 (2021) 103964.
- [7] K. Nonami, R. K. Barai, A. Irawan, M. R. Daud, *Hydraulically actuated hexapod robots*, Springer Japan (2014).
- [8] M. D. Teji, T. Zou, D. S. Zeleke, A survey of off-road mobile robots: Slippage estimation, robot control, and sensing technology, *Journal of Intelligent & Robotic Systems* 109 (2) (2023) 38.
- [9] Y. Hao, L. Quan, S. Qiao, X. Lianpeng, X. Wang, Coordinated control and characteristics of an integrated hydraulic–electric hybrid linear drive system, *IEEE/ASME Transactions on Mechatronics* 27 (2) (2021) 1138–1149.
- [10] J. Wang, Z. Liu, H. Chen, Y. Zhang, D. Zhang, C. Peng, Trajectory tracking control of a skid-steer mobile robot based on nonlinear model predictive control with a hydraulic motor velocity mapping, *Applied Sciences* 14 (1) (2023) 122.
- [11] J. Wang, S. Gao, K. Wang, Y. Wang, Q. Wang, Wheel torque distribution optimization of four-wheel independent-drive electric vehicle for energy efficient driving, *Control Engineering Practice* 110 (2021) 104779.
- [12] W. Lee, M. J. Kim, W. K. Chung, Model-free joint torque control strategy for hydraulic robots, in: 2016 IEEE International Conference on Robotics and Automation (ICRA), IEEE, 2016, pp. 2408–2415.
- [13] H. Yin, H. Xu, W. Fan, F. Sun, Fault diagnosis of pressure relief valve based on improved deep residual shrinking network, *Measurement* 224 (2024) 113752.
- [14] C. P. Vo, H. V. Dao, K. K. Ahn, et al., Robust fault-tolerant control of an electro-hydraulic actuator with a novel nonlinear unknown input observer, *IEEE Access* 9 (2021) 30750–30760.
- [15] R. Galati, G. Mantriota, G. Reina, Adaptive heading correction for an industrial heavy-duty omnidirectional robot, *Scientific Reports* 12 (1) (2022) 19608.
- [16] L. Chen, Z. Qin, M. Hu, H. Gao, Y. Bian, B. Xu, X. Peng, Trajectory tracking control of autonomous heavy-duty mining dump trucks with uncertain dynamic characteristics, *Science China Information Sciences* 66 (10) (2023) 202203.
- [17] A. Nagariya, S. Saripalli, An iterative lqr controller for off-road and on-road vehicles using a neural network dynamics model, in: 2020 IEEE Intelligent Vehicles Symposium (IV), IEEE, 2020, pp. 1740–1745.
- [18] J. Wang, M. T. Fader, J. A. Marshall, Learning-based model predictive control for improved mobile robot path following using gaussian processes and feedback linearization, *Journal of Field Robotics* 40 (5) (2023) 1014–1033.
- [19] B. Zhang, Y.-H. Chen, Y. Jia, J. Huang, D. Yang, Z. Zhong, Accuracy and safety: tracking control of heavy-duty cooperative transportation systems using constraint-following method, *IEEE Transactions on Intelligent Transportation Systems* (2024).
- [20] F. Gauthier-Clerc, A. Hill, J. Laneurit, R. Lenain, E. Lucet, Online velocity fluctuation of off-road wheeled mobile robots: A reinforcement learning approach, in: 2021 IEEE International Conference on Robotics and Automation (ICRA), IEEE, 2021, pp. 2421–2427.
- [21] J. Knaup, K. Okamoto, P. Tsiotras, Safe high-performance autonomous off-road driving using covariance steering stochastic model predictive control, *IEEE Transactions on Control Systems Technology* (2023).
- [22] Y. Liu, T. Li, J. Duan, X. Wu, H. Wang, Q. Fan, J. Lin, Y. Hu, On a hierarchical adaptive and robust inverse dynamic control strategy with experiment for robot manipulators under uncertainties, *Control Engineering Practice* 138 (2023) 105604.
- [23] P. Yu, Y. Zhou, X. Sun, H. Sang, S. Zhang, Station-keeping strategy for wave gliders considering obstacle area, *Control Engineering Practice* 153 (2024) 106093.
- [24] J. Liao, Z. Chen, B. Yao, Model-based coordinated control of four-wheel independently driven skid steer mobile robot with wheel–ground interaction and wheel dynamics, *IEEE Transactions on Industrial Informatics* 15 (3) (2018) 1742–1752.
- [25] G. R. Petrović, J. Mattila, Analytic solutions for wheeled mobile manipulator supporting forces, *IEEE Access* 10 (2022) 43235–43255.
- [26] M. Jelali, A. Kroll, *Hydraulic servo-systems: modelling, identification and control*, Springer Science & Business Media, 2012.
- [27] L. Hulttinen, J. Mattila, Model-based control of a mobile platform with independently controlled in-wheel hydraulic motors, *Journal of Fluid Power Systems Technology* 85239 (2021) V001T01A001.
- [28] M. Inderelst, H. Murrenhoff, Hydraulic proportional and servo valves, in: T. Mang (Ed.), *Encyclopedia of Lubricants and Lubrication*, Springer, Berlin, Heidelberg, 2014, pp. 1–8.
- [29] M. Corless, G. Leitmann, Bounded controllers for robust exponential convergence, *Journal of Optimization Theory and Applications* 76 (1) (1993) 1–12.
- [30] M. Heydarishahna, M. Bahari, J. Mattila, Robust observer-based control with modularity and exponential stability for interconnected systems, *arXiv preprint arXiv:2311.15843* (2023).
- [31] M. Heydari Shahna, M. Bahari, J. Mattila, Robust decomposed system control for an electro-mechanical linear actuator mechanism under input constraints, *International Journal of Robust and Nonlinear Control* (2024).
- [32] M. H. Shahna, M. Abedi, Design of a finite time passivity based adaptive sliding mode control implementing on a spacecraft attitude dynamic simulator, *Control Engineering Practice* 114 (2021) 104866.
- [33] N. Deniz, F. Jorquera, M. Torres-Torriti, F. A. Cheein, Model predictive path-following controller for generalised n-trailer vehicles with noisy sensors and disturbances, *Control Engineering Practice* 142 (2024) 105747.
- [34] J. Cai, C. Wen, H. Su, Z. Liu, L. Xing, Adaptive backstepping control for a class of nonlinear systems with non-triangular structural uncertainties, *IEEE Transactions on Automatic Control* 62 (10) (2016) 5220–5226.
- [35] J. Schwarz, B. Lohmann, Robust identification and control of mobile hydraulic systems using a decentralized valve structure, *Control Engineering Practice* 151 (2024) 106030.
- [36] M. H. Shahna, J. Mattila, Model-free generic robust control for servo-driven actuation mechanisms with layered insight into energy conversions, *arXiv preprint arXiv:2409.11828* (2024).
- [37] B. Ren, S. S. Ge, K. P. Tee, T. H. Lee, Adaptive neural control for output feedback nonlinear systems using a barrier lyapunov function, *IEEE Transactions on Neural Networks* 21 (8) (2010) 1339–1345.
- [38] M. H. Shahna, S. A. A. Kolagar, J. Mattila, Integrating deepRL with robust low-level control in robotic manipulators for non-repetitive reaching tasks, in: 2024 IEEE International Conference on Mechatronics and Automation (ICMA), IEEE, 2024, pp. 329–336.